Proceedings of ASME Turbo Expo 2022
Turbomachinery Technical Conference and Exposition
GT2022
June 13-17, 2022, Rotterdam, The Netherlands

GT2022-82128

NUMERICAL PREDICTION OF HEAT TRANSFER COEFFICIENT AND ADIABATIC EFFECTIVENESS ON A NOZZLE GUIDE VANE WITH REPRESENTATIVE COMBUSTOR OUTFLOW

S.G. Tomasello, A. Andreini, T. Bacci, B. Facchini
Department of Industrial Engineering
University of Florence
Florence, Italy
stellagrazia.tomasello@unifi.it

S. Cubeda, L. Andrei
Baker Hughes
Florence, Italy
simone.cubeda@bakerhughes.com

ABSTRACT

The employment of lean-premix combustors in modern gas turbines allows to reduce NOx emissions by controlling the flame temperature at the expense of highly unsteady and strongly non-uniform flow fields which are necessary to stabilize the flame. This highly complex swirled flow field characterized by evident temperature distortions alters the aerodynamics and heat transfer in the first high pressure turbine stator with potential detrimental consequences on engine life and efficiency. From a numerical point of view, the mutual combustor-turbine interaction has been studied by using standard turbulence modeling approaches, as commonly employed during the design phase, even if more advanced scale-resolving methods have been proven more reliable and benchmarked against various experimental findings.

From the experimental perspective, film-cooling adiabatic effectiveness and heat transfer coefficient (HTC) measurements on the external surface of the nozzle guide vanes, in the presence of representative combustor outflow characteristics, are not common since the relevant temperature distortions that are present make such kind of measurements really challenging to perform. For this reason, very limited assessment of such approaches regarding this aspect is available in literature.

In this study, an experimental test case with a combustor simulator and a nozzle cascade, where both adiabatic effectiveness and HTC measurements have been carried out, is investigated by carrying out a systematic computational study, through RANS calculations of the combustor-cascade integrated domain. The film cooling system performance has been predicted by meshing the whole vane internal cooling system, while the heat transfer coefficient is calculated using the conventional two-point method, normally adopted for heat transfer calculations in gas turbines.

The comparison between numerical predictions and experimental results was exploited to assess the capability of traditional modeling approaches in the characterization of both adiabatic effectiveness and heat transfer coefficient. This evaluation represents an effective means to assess if conventional/industrial approaches can be reliably used, when representative and highly unsteady combustor outflows are considered, or advanced and more time-consuming methods shall be adopted.

Keywords: Gas turbine, Combustor, Turbine, Interaction, Swirling flow, CFD, RANS, Experiments, HTC, PSP.

NOMENCLATURE

C	Concentration
p	Pitch [mm]
P	Pressure [Pa]
q	Heat flux
T	Temperature [K]
y^+	Non-dimensional first cell wall distance [-]

Subscripts

ad	Adiabatic
ax	Axial
aw	Adiabatic wall
cool	Relative to the coolant
fg	Foreign gas
nd	Non-dimensional
rad	Radial
ref	Reference value
t	Total quantity
tan	Tangential
TC	ThermoCouple
w	Relative to the wall

Acronyms

LE	Leading Edge
FRTC	Fast Response ThermoCouple
HPT	High Pressure Turbine
HTC	Heat Transfer Coefficient
NGV	Nozzle Guide Vane
PS	Pressure Side

PSP	Pressure Sensitive Paints
RANS	Reynolds-Averaged Navier Stokes
SS	Suction Side

Greek letters

η	Film-cooling adiabatic effectiveness

INTRODUCTION

The combustor-turbine interaction has been studied since the last three decades, thanks to the exploitation of dedicated experimental test rigs. These were first realized in the US by NASA [1], the United Technologies Research Center [2], the MIT [3], the Air Force Research Laboratory [4] as well as the Universities of Texas [5]. More lately also in Europe facilities were equipped to investigate over this topic, especially, in the UK by QinetiQ [6] and Oxford [7] [8] [9] and in Germany by Darmstadt TU [10].

The necessity for such thorough investigations is becoming more and more impelling due to the emerging combustion technologies and, in particular, to the passage from Rich-Quench-Lean (*RQL*) to lean-burn combustion systems. Due to this, the focus has moved from the interaction between the unsteady main flow and liner cooling flows to the impact of a highly swirled and temperature-distorted main flow field on the turbine nozzle guide vanes. In fact, a more limited amount of air is available for liner cooling purposes and dilution holes, typical of RQL architectures, are not employed in lean combustors. Therefore a much more limited interaction between main anc coolant flos occurs. This finally results in a highly-swirled, for flame stabilization reasons, and temperature-distorted flow field at the High Pressure Turbine (*HPT*) inlet, as well shown both numerically and experimentally by Cha et al. [11] [12] and also by Shih et al [13] and by Lin et al. [14], who studied the impact of the inlet swirl angle on the flow and heat transfer on nozzle vanes.

The effects of an inlet swirl profile on film-cooling adiabatic effectiveness have not been widely studied through experimental approaches. Giller and Schiffer [15] have analyzed the swirl-induced adiabatic effectiveness distribution on the *LE* of a stator vane in a linear cascade, finding the alteration of the stagnation line position and hence of the film-cooling holes working conditions. Werschnik et al. [16] have as well found a reduced degree of protection on film-cooled endwalls in the presence of highly-swirled inflows.

The evaluation of the heat transfer coefficient (*HTC*) on the airfoil surfaces, on the other hand, is one further aspect of great importance and has indeed been investigated in the presence of swirled combustor outflows by authors such as Qureshi et al. [17]. They have shown how swirl-induced alteration of the stagnation line and secondary flows evolution can lead to lower/higher heat transfer regions than with uniform inflow.

Even if in the recent years *CFD* is constantly improving in the accurate replication of physical phenomena, complex researches are still being conducted through experiments, useful to tune, refine and validate numerical models.

Within the combustor-turbine interaction context, the recent FACTOR project ('Full Aerothermal Combustor-Turbine interactiOn Research') [18] has represented a very important test case and a database for analyzing the impact of a lean-burn combustion system over a 1.5 stage high-pressure turbine. The smaller rig replica installed at the 'Technology for High Temperature' (*THT*) laboratory of the University of Florence, [19] was thoroughly employed through Particle Image Velocimetry (*PIV*, for the flow field) and Pressure Sensitive Paints (*PSP*, for the film coverage) [20]. The rig was capable to reproduce the presence of both temperature distortion and aggressive swirled flow field, even in non-reactive conditions. Such accurate test data allowed for the exploitation of advanced *CFD* methodologies based on scale resolving simulations, as carried out by CERFACS [21] and the University of Florence [22] [23], who have proven the importance of integrated approaches for the sake of achieving high-fidelity predictions of the aerothermal field at the turbine entrance. On the other hand, these approaches are well known to be significantly expensive, in terms of computational time and cost, and therefore, not well suited for industrial design practice.

Lastly, the necessity for increasing the knowledge on combustor-turbine interaction and improving standard design practices for industrial applications has led to the design and installation of a new test rig representative of a heavy-duty configuration and hosting real components. The steps taken during the design of such rig were described by Cubeda et al. [24], who made use of both steady and unsteady simulations.

The scope of the present work is to illustrate the comparison between numerical and experimental results relatively to the film-cooling adiabatic effectiveness and the external heat transfer coefficient (*HTC*) over the airfoil surface, which are of major importance in the design of *HPT* nozzle guide vanes.

RANS approaches were used, in order to assess the capabilities of the more common industrial tools for the prediction of the above mentioned phenomena, under representative combustor outflow conditions. A very limited number of studies have been carried out, with this kind of EXP-CFD benchmarking, due to the very limited amount of experimental data in these conditions. Experimental results are also subject for separate publications by Bacci et al. [25] and Babazzi et al. [26] and represent the basis of comparison for the present study.

TEST RIG DESIGN AND CHARACTERISTICS

The aforementioned test rig is a lean-burn combustor simulator which very closely mimics the real engine configuration of a Baker Hughes' heavy-duty gas turbine, yet working in non-reactive conditions in order to allow the ease of installation and operation and, at the same time, to carry out detailed measurements.

The 3D layout model of the rig, partly including real hardware, is shown in FIGURE 1a. The mainflow is introduced in the combustion chamber through three lean-premixed burners, at the exit section of which cylindrical ducts were installed as to ensure a representative swirling flow at the combustor-turbine interface plane. This turned to be necessary

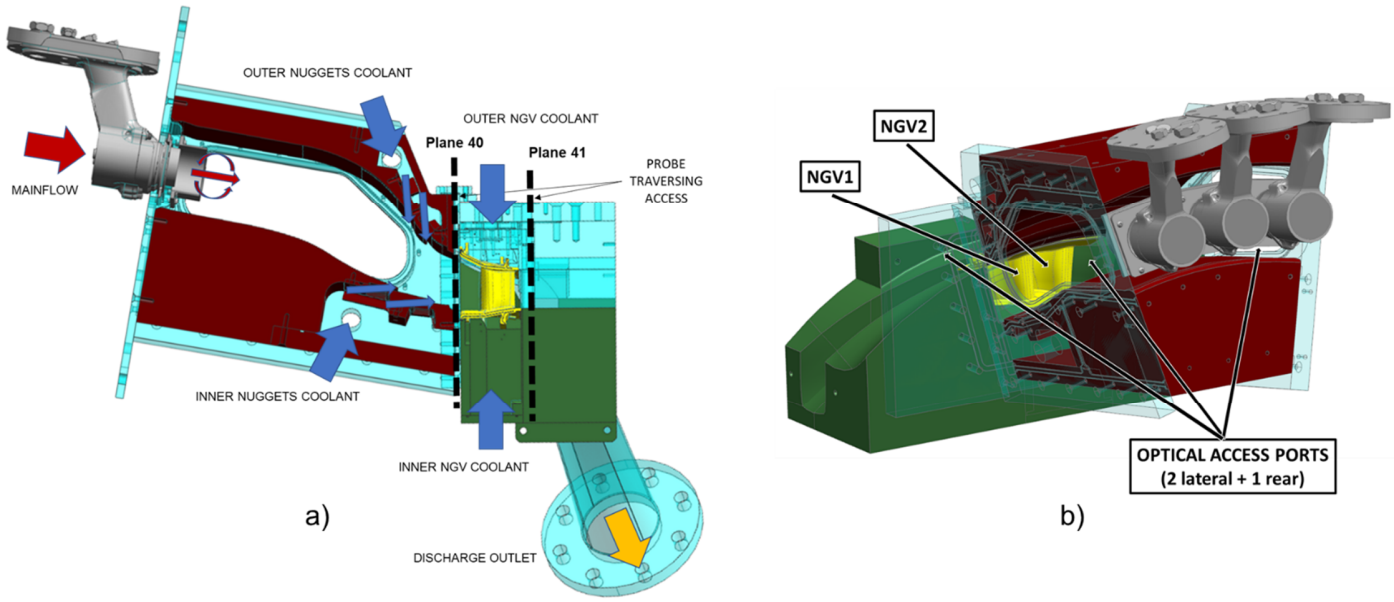

FIGURE 1: TEST RIG 3D LAYOUT (a) AND OPTICAL ACCESS DETAILS (b) (© 2022 Baker Hughes Company – All rights reserved)

during the early stages of the project, due to the non-reactive conditions at which the rig is operated, as also performed in other works with similar goals [27] [28]. According to the working condition under test, the mainflow can undergo a temperature increase through an electrical heater installed upstream of the swirlers.

In addition to combustor representative high-swirl characteristics, the flow field at the turbine inlet can also get temperature-distorted by means of liner cooling nuggets (2x on the outer, 2x on the inner surface), i.e. 2D slot-cooling, located in the final part of the chamber and fed by ambient air.

The nozzle guide vanes (*NGV*) cascade is composed by two vanes and three passages. The module was designed in the early stage of the project [24] via *CFD* as per a design of experiments approach. Through this, the sidewalls were built in order to replicate the target conditions of a periodic simulation on the central vane passage, also considering that there was not a 1:1 ratio between swirler and nozzle real components.

The rig is equipped of instrumentation accesses for probe traversing measurements across the nozzles cascade, i.e. at both Plane 40 and Plane 41 (see FIGURE 1a) and, additionally, three optical access ports are present as illustrated in FIGURE 1b. The two lateral accesses are useful to alternately investigate the front part of the pressure side (*PS*) of *NGV2* or the leading edge (*LE*) and front part of the suction side (*SS*) of *NGV1*, while the rear port is used for the final part of the *SS* of *NGV1*.

Concerning the experimental activity, which is thoroughly described in separated works and it is not the object of the present publication, several test campaigns were carried out to detail the NGV inlet/outlet aerothermal field and turbulence intensity, using five-hole-probe and hot wire anemometry traversing respectively. Measurements were also carried out on the NGV surface to characterize the adiabatic effectiveness generated by the film-cooling system and the external heat transfer coefficient, on a solid vane airfoil (i.e. with out film-cooling holes). The first aspect was retrieved through PSP (Pressure Sensitive Paint) technique, exploiting heat and mass transfer analogy and tracing an oxygen-free gas that was used to feed the film cooling flows. This technique also allowed to evaluate the pressure distribution on the airfoils, thus assessing the vane loads. HTC and adiabatic wall temperature measurements on the other hand were carried out through a transient thermal approach where the vane surface temperature rise is tracked, by means of an infra-red (*IR*) camera, once a sudden temperature step is provided to the swirler flow, through the activation of a fast heater. Film-cooled nozzles were obviously employed for the adiabatic effectiveness test, whereas a non-cooled *NGV* doublet, with the same airfoil profile of the former and made by a low thermal-diffusivity and high-temperature resistant material (polyether ether ketone "peek"), was adopted for measuring the external *HTC*. Additional and detailed information regarding both techniques' methods, post-processing approaches and accracy evaluations can be found in [25] and [29]. Glass windows were employed for *PSP* measurements, while sapphire windows were needed to frame the target with the IR camera and derive *HTC* and adiabatic wall temperature for the non film-cooled case.

The operating conditions of the rig, used for stationary, probe traversing tests on Plane 40 and 41 are derived from the nominal ones [24], which were scaled from real engine conditions in order to conserve the Mach number. By contrast, it was not possible to simultaneously fulfill the Reynolds number similitude due to facility constraints, yet the rig achieves representative conditions for secondary flows and pressure loss mechanisms, although heat transfer rates are slightly reduced.

PSP and *HTC* tests, however, were conducted in purposely different operating conditions, reported in TABLE 1, due to measurement techniques constraints. In particular, for the former all flows had to be kept at room temperature. Since the aero-field is not altered by swirler temperature variation and a still representative turbine temperature ratio (≈1.5) was achieved by using CO2 for film-cooling flows, PSP results must be expected to be well representative of the adiabatic effectiveness generated in design point conditions. PSP measurement uncertainty is quite limited, generally within 10% for low values of adiabatic effectiveness (≈0.2) and 2% for higher ones (>0.8). Concerning HTC tests, on the other hand, the mainstream temperature is actually increased to the nominal value (533.15 K), while cooling flows stay at ambient temperature. Note that, however, some heat conduction phenomena cannot be avoided due to the metallic material of most of the rig, which leads to some temperature rise in the nuggets flow temperature as reported in TABLE 1, yet not compromising the validity and representativeness of the test. The operating conditions for the numerical calculations were precisely chosen to resemble to ones from experiments, so they differ between runs carried out to predict adiabatic effectiveness and HTC results, as described previously.
It must be also pointed out that HTC tests are carried out in transient conditions, which implies a slightly higher temperature reduction through the chamber with respect to steady tests/CFD. The experimental uncertainty was estimated to stay within ±13% for heat transfer coefficient and ±3K for adiabatic wall temperature measurements.

TABLE 1: OPERATING CONDITIONS (© 2022 Baker Hughes Company – All rights reserved)

	PSP test	**HTC test**
Combustion chamber		
Re_m @ Plane 40 [-]	1.65E+05	1.17E+05
Ma_m @ Plane 40 [-]	0.074	0.074
Swirler temperature [K]	300	533.15
Nuggets flow temperature [K]	300	325
Swirler-nuggets flow split [%]	85-15	85-15
Turbine		
NGV throat Mach number [-]	0.79	0.67
Film-cooling temperature [K]	300	-
Film/Plane 40 mass flow ratio [%]	13.6	-

NUMERICAL SETUP

Simulations were performed using ANSYS CFX v19.4, with the selected algorithm being pressure-based with Rhie-Chow pressure-velocity coupling. In agreement with the best practices specified by the software developers [30], all equations are discretized with the "high resolution" scheme. Turbulence is modelled using the k-ω SST model by Menter, then an automatic near-wall treatment guarantees the blending between wall-function and wall-integration application based on the local y^+ value, not always lower than 1 due to geometrical and computational constraints.

The simulation domain is the one reported in FIGURE 2. The hybrid unstructured computational grid, reported in FIGURE 3, was generated with ANSYS Meshing and is composed of 14 prismatic layers and filled with tetrahedra. The mesh counts $99 \cdot 10^6$ elements. A 1.5 mm characteristic size was adopted within the injectors, which is reduced to 1 mm in the refinement region right downstream of the swirlers, while the y^+ value keeps below 5 all over the blade surface. The mesh sizing is compatible with the one used in the analysis of a similar configuration with non-uniform inlet profiles and a couple of fully covered cooled vanes [31].

Mass flow boundary conditions were prescribed at all inlet sections, leveraging experimental data, while static pressure was imposed at the domain's outlet. Furthermore, the proper expansion ratio through the *NGV* cascade was controlled via comparing the static pressure at specified locations on the outer endwall with pressure probe measurements. All walls were treated as no slip and smooth surfaces.

Finally coming to the adopted operating conditions, the *PSP* case was replicated straight from the scenario reported in TABLE 1, yet reminding that *PSP* by nature retrieve an averaged distribution of film-cooling adiabatic effectiveness based on stabilized flow conditions. From the numerical standpoint, the internal cooling system of the tested vane was meshed and resolved, in order to provide an accurate modeling of the film-cooling behavior. While the meshed internal cooling system can not be shown, due to proprietary reasons, it can be stated that this resulted in a non-negligible increase in the computational cost of the domain, bringing the total mesh elements number to about $169 \cdot 10^6$.
To track film cooling concentration, a passive scalar was introduced, assigning a value equal to 1 at the inlets of the internal channels and 0 at the combustor outlet flow; in this way it was possible to retrieve adiabatic effectiveness values, based on concentration measurements, as it is done by PSP, capitalizing on heat and mass transfer analogy.On the contrary, as anticipated, it was not possible to strictly reproduce the exact *HTC* test case, due to the inherent transient approach of the technique. In fact, reproducing such a "long" duration (20s) experiment through *CFD* would be impractical for time consumption and/or resource demands, given the very small time step required to ensure an appropriate Courant number in the swirling region and especially through the nozzles, where the highly accelerating flow would call for an even finer mesh.

For this reason and according to the purpose of this activity, the heat transfer coefficient was calculated using the conventional two-point method, normally adopted for heat transfer calculations in gas turbines. This consists in performing two simulation runs in series:

- The first is adiabatic, from which the adiabatic wall temperature (T_{aw}) on the airfoils surface is retrieved;
- The second is then carried out by imposing a specified wall temperature, equal to T_{aw} detracted by an arbitrary ΔT (150K in this case), which determines a wall heat flux q_w.

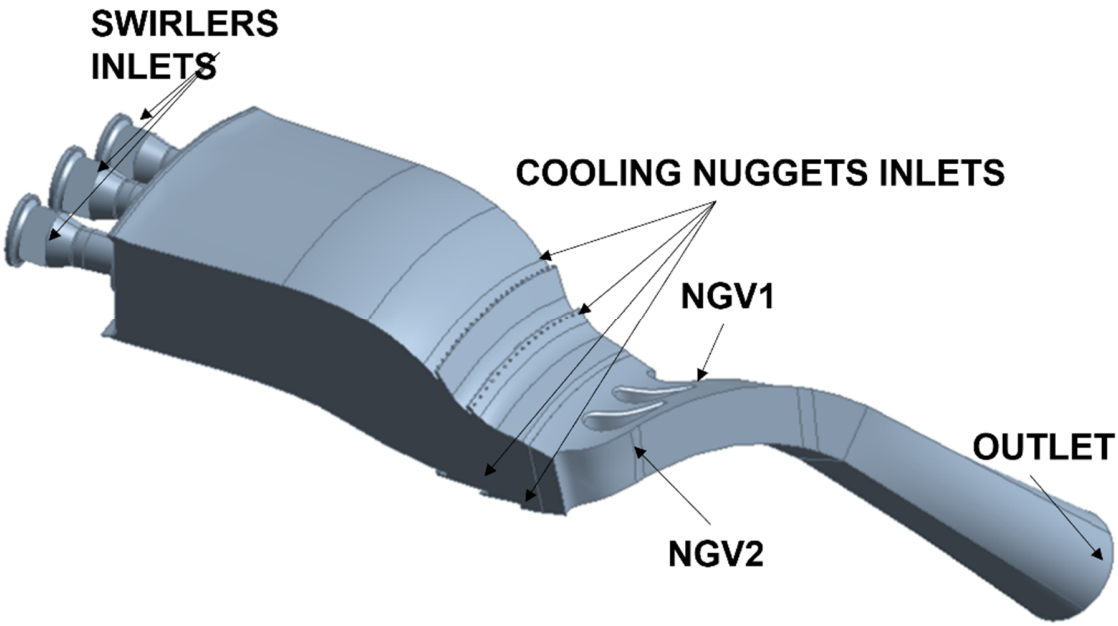

FIGURE 2: COMPUTATIONAL DOMAIN OF COMBUSTOR+NOZZLES RIG(© 2022 Baker Hughes Company – All rights reserved)

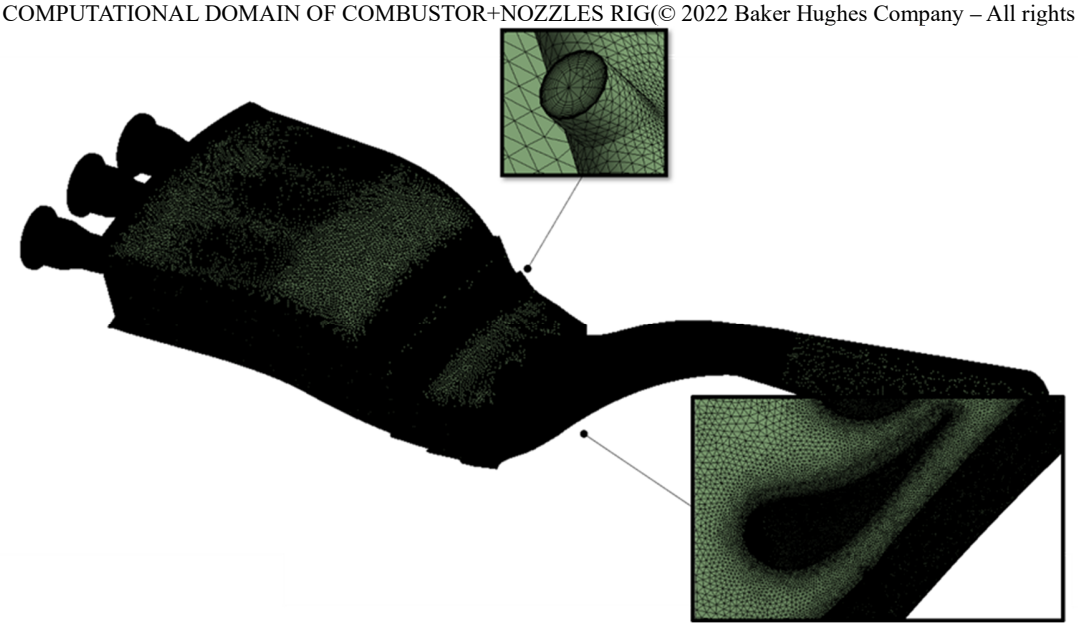

FIGURE 3: COMPUTATIONAL GRID OF THE COMBUSTOR+NOZZLES DOMAIN (© 2022 Baker Hughes Company – All rights reserved)

Eventually, the *HTC* is evaluated at any location as per the following expression:

$$HTC = \frac{q_w}{T_{aw} - T_w} = \frac{q_w}{\Delta T} \qquad (1)$$

RESULTS

Boundary conditions

Before showing the comparison between experimental data and numerical predictions of film-cooling adiabatic effectiveness and heat transfer coefficient on the airfoils surface, it is worth checking that the major flow field quantities at the combustor-turbine interface as estimated by *CFD* simulations are in line with measurements. FIGURE 4 reports on the left-hand column the measurements obtained by means of a five-hole probe traversing at Plane 40 with the rig being operated in warm conditions (i.e. design point or equivalently for the *HTC* test), while on the right-hand one the corresponding aerothermal field quantities obtained via *CFD*.

In particular, the swirl, pitch, non-dimensional total temperature ($T_{t,nd}$) and pressure fields are shown in sequence on

each row of the figure. Note that on the x-axis of the plots is the t/p_{NGV}, i.e. the tangential-angle to the angular *NGV*-pitch ratio, whereas on the y-axis the normalized *NGV* height *h/H* (or span) is reported. Swirl, pitch and $T_{t,nd}$ are defined as follows:

$$swirl = \frac{V_{tan}}{V_{ax}} \tag{2}$$

$$pitch = \frac{V_{rad}}{V_{ax}} \tag{3}$$

$$T_{t,nd} = \frac{T_t - T_{nuggets}}{T_{swirler} - T_{nuggets}} \tag{4}$$

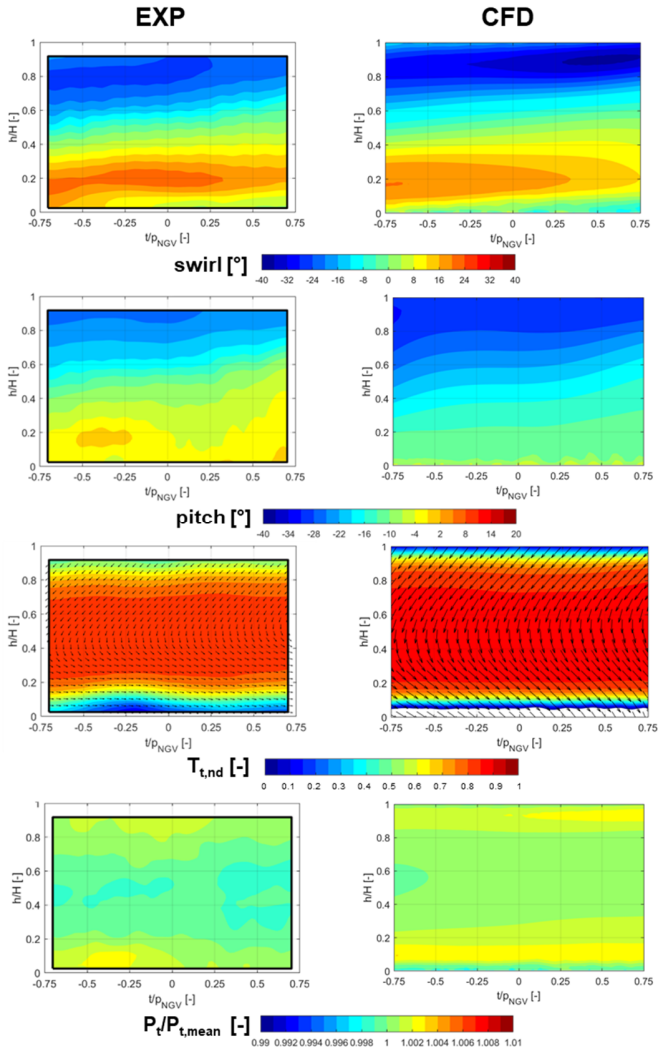

FIGURE 4: FIVE-HOLE PROBE AND CFD CONTOURS AT PLANE 40 (© 2022 Baker Hughes Company – All rights reserved)

The present comparison at Plane 40 shows a satisfactory match with respect to the experimental maps. This is especially true for what concerns the swirl, total temperature and pressure field, whereas some discrepancy is still evident in the pitch distribution. The match on swirl is to be stressed, since it is the main driver for the hot streak propagation through the stator. Moreover, it is responsible for altering the flow impacting on the nozzles, thus potentially affecting both the film-cooling system coverage and the *HTC* distribution.

The verification of proper boundary conditions included, as already mentioned, also the check on the outer endwall pressure distribution at Plane 41, where pressure taps are placed. FIGURE 5 compares the experimental readings to the values estimated via *CFD*. Part of the rig section shape is also reported to more clearly indicate the taps positioning.

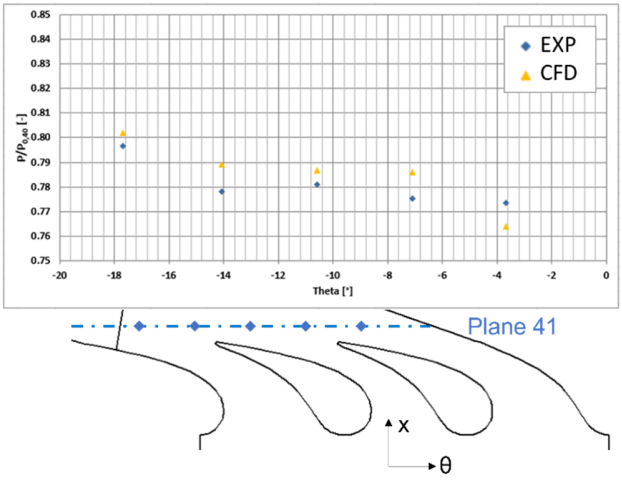

FIGURE 5: PRESSURE DISTRIBUTION ON THE OUTER ENDWALL OF PLANE 41 (© 2022 Baker Hughes Company – All rights reserved)

The pressure distribution obtained via *CFD* falls very close to experimental data, with some overprediction at all pressure taps locations, except for the right-most one, where some overexpansion is modelled by the *CFD*, whereas this is not present in measurements. More accurate results can be pursued by improving the match with experimental data at the combustor-turbine interface as well as across the vane passage via the use of more advanced *CFD* modelling.

Now coming to the core of the present activity's scope, which is the impact of representative combustor outflow on the nozzles aero-thermal performance, it is convenient to focus on the airfoils.As per their name, pressure sensitive paints (*PSP*) can be first of all employed to retrieve the pressure distribution over the given tested surface. Thus, *CFD* results can be benchmarked against experimental measurements as shown in FIGURE 6. Note that the "red" and "blue" frames are taken from the two lateral ports positioned respectively on the left and right sides of the rig based on a forward-looking-aft view, while the "green" frame is shot from the rear port, which looks at the airfoils *SS* downstream of the throat section. In both cases, the pressure distribution is fairly uniform in the first part of the *PS* (frame 1), while on the *SS* (frame 2 and 3) the pressure gradient is more pronounced, especially where the throat section is crossed.

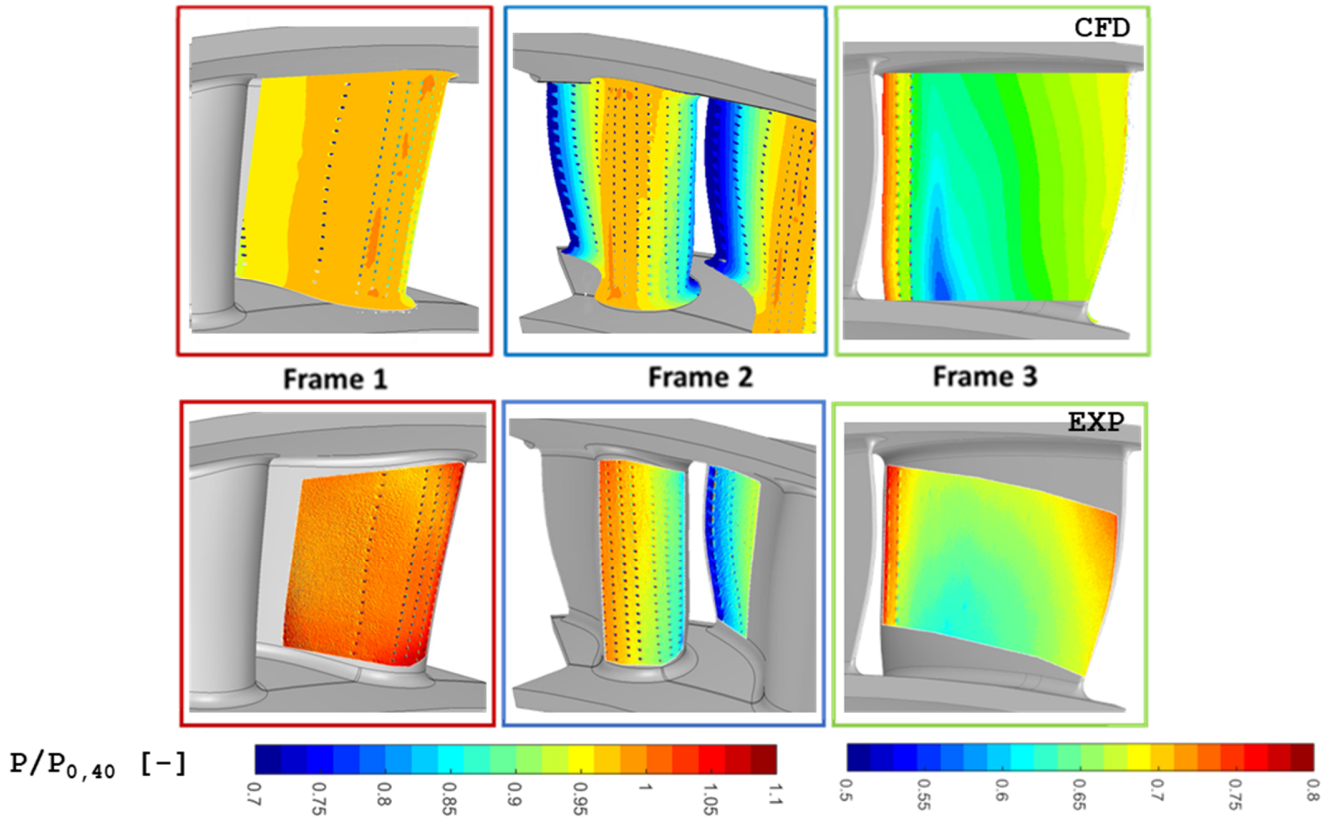

FIGURE 6: NOZZLES PRESSURE DISTRIBUTION (PSP EXP vs CFD) (© 2022 Baker Hughes Company – All rights reserved)

The comparison can then be extended to the blade load curves at a certain span section of the airfoil, which, per the mid-span, is reported in FIGURE 7.

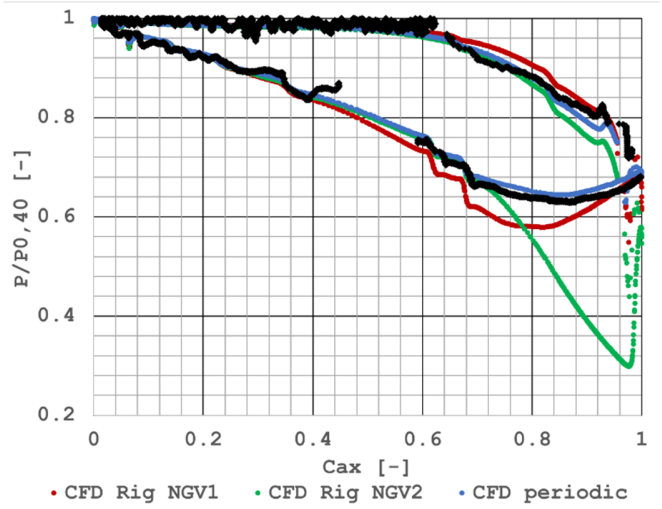

FIGURE 7: NOZZLES PRESSURE LOAD) (© 2022 Baker Hughes Company – All rights reserved)

The experimental curves indicate a significant measurement noise, due to the low sensitivity of the measurement technique to pressure measurements [24]. *CFD* results bring a satisfactory match with measurements, if focusing on the central vane passage, i.e. on the *SS* of *NGV1* and the *PS* of *NGV2*, which, by the way, complies with the original design intent. In fact, note that in the same graph also the *CFD* periodic case (sole *NGVs*), carried out during the rig design phase, is included, to emphasise the representativeness of the rig with respect to a real engine arrangement, where no tailboard is obviously present.

Film-cooling adiabatic effectiveness

As already anticipated, *PSP* are an effective mean to measure the film-cooling adiabatic effectiveness, being a concentration detector. Dealing with film-cooled nozzles, the adiabatic effectiveness is the major indicator of the cooling system performance, since it judges over its ability to cover and protect the nozzles surface.

The comparison between numerical predictions and experiments is illustrated in FIGURE 8, for the three reference frames, corresponding to the available optical accesses as shown in FIGURE 1a. Frames reference is the same as for FIGURE 6. If focusing on one single frame at a time, some more detailed considerations can be derived. Starting from the *LE* region (frame 2), the experimental map returns a non-straight stagnation line, since two low effectiveness areas are spotted.

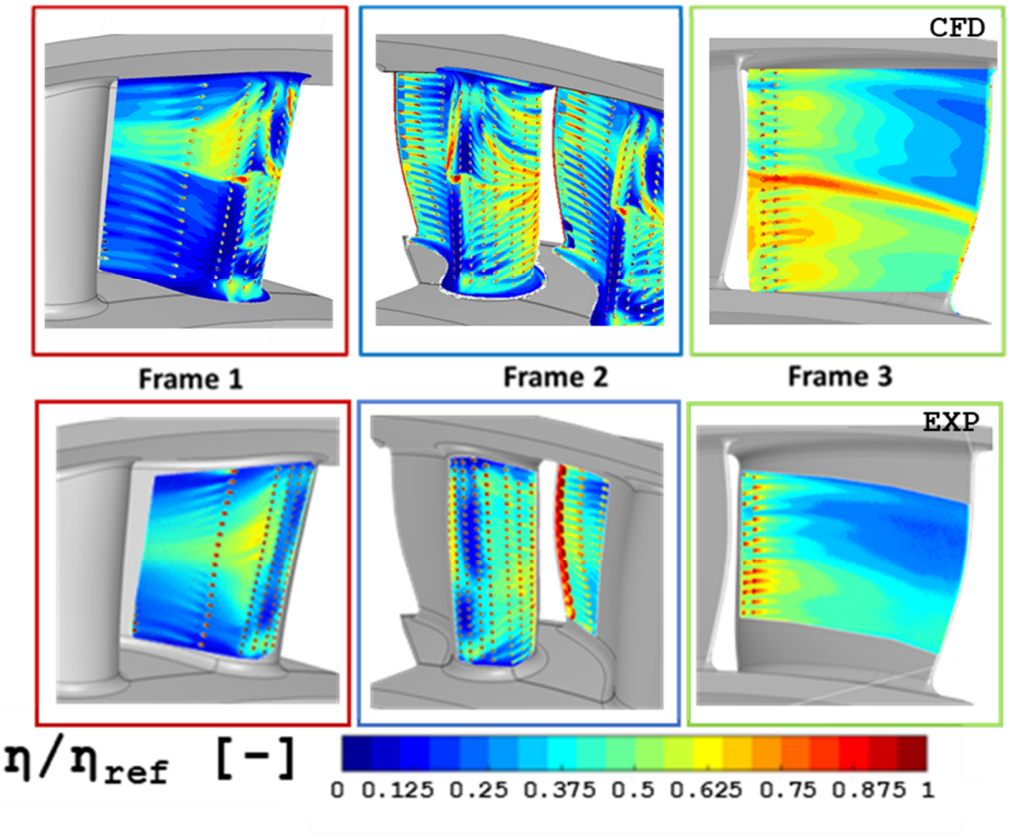

FIGURE 8: FILM-COOLING ADIABATIC EFFECTIVENESS (© 2022 Baker Hughes Company – All rights reserved)

This phenomenon, induced by the highly-swirled impacting flow, is partly captured by *CFD*, where coolant traces are slightly more isolated than the experimental map. Moreover, measurements indicate the position of the stagnation line to be moved slightly more downstream on the *SS* than what predicted by the *CFD*.

Then the *PS* (frame 1) and *SS* (frame 3) undergo diametrically opposite behaviours. In fact, due to the swirled main flow structure, a better film coverage is attained in the higher half of the *PS* and the lower half of the *SS*. The highest protection is achieved close to the midspan, where the coolant traces look more intense, which is likely driven by the low-pressure core of the main-flow.

This behaviour can be attributed to the RANS modelling, since it is known how its associated strong underprediction of the turbulent mixing can lead to a different distribution of the adiabatic effectiveness along the vane compared to the experimental data, leaving areas of the vane locally unprotected (such as the lower half of the pressure side) while overpredicting the effectiveness in others (such as the higher half of the pressure side). This phenomenon has been observed also in previous works of the authors [23] [32].

To have a further and more quantitative appreciation of the differences between experiments and RANS predictions line plots of the film-cooling adiabatic effectiveness have been reported in FIGURE 9. FIGURE 9a shows an extraction at a given axial location on the PS, whereas FIGURE 9b on the NGV SS surface, with profiles of the normalized adiabatic effectiveness (x-axes) along with the nozzle span (y-axes).

Such comparison on the PS surface highlights how the CFD predicts a net separation of coolant distribution between the higher and lower half, which is induced by the swirled inflow but is not as sharp in the experimental measurements. On the other hand, on the SS the comparison holds on a more restricetd portion of the surface due to accessibility constraints. Despite this fact, numerical and experimental values are comparable on the higher span-fraction, while an intense accumulation of coolant is predicted by the CFD, which however and as mentioned is in line with previous literature findings. Some higher coolant presence and hence less mixing is also predicted on the lower span-fraction, which in both CFD and measureaments is however specular to the distribution on the pressure side as dictated by the impacting swirling flow.

As a consequence, it can be stated that *CFD* is satisfactorily replicating the coolant alternate spread on the higher/lower half of the *PS*/*SS* due to the main flow swirling structure, although there is yet wide margin for improvement. In fact, based on available data in the open literature, it is expected that more advanced CFD modelling techniques (such as scale-resolving methods) can help in overcoming the limitations of RANS in accurately reproducing the mixing between coolant and main streams [23] [32].

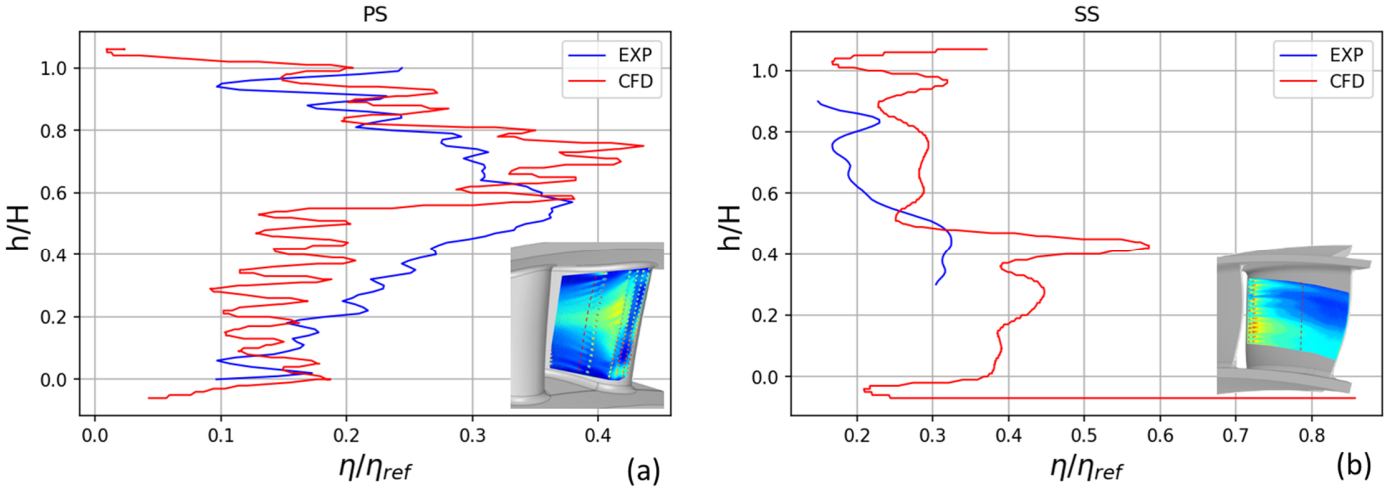

FIGURE 9: FILM-COOLING ADIABATIC EFFECTIVENESS EXTRACTED AT A GIVEN AXIAL POSITION ON THE PS (a) AND SS (b) SURFACES (© 2022 Baker Hughes Company – All rights reserved)

Heat transfer coefficient

The comparison between measured and numerically evaluated heat transfer coefficient is reported in FIGURE 10, with the same frames reference adopted so far. Note that *HTC* values were non-dimensionalized with respect to a reference *HTC* (HTC_{ref}), which is the maximum value at the airfoil nose.

Looking at the experimental maps, the maximum *HTC* is found on the airfoil *LE* (frame 2) at around 0.25 span fraction and slightly shifted towards the *PS* (frame 1). Sticking to frame 2, it is possible to notice that the actual stagnation line (continuous) is deviating in a "twist" fashion with respect to the geometrical one (dashed) due to the superimposed inlet swirl.

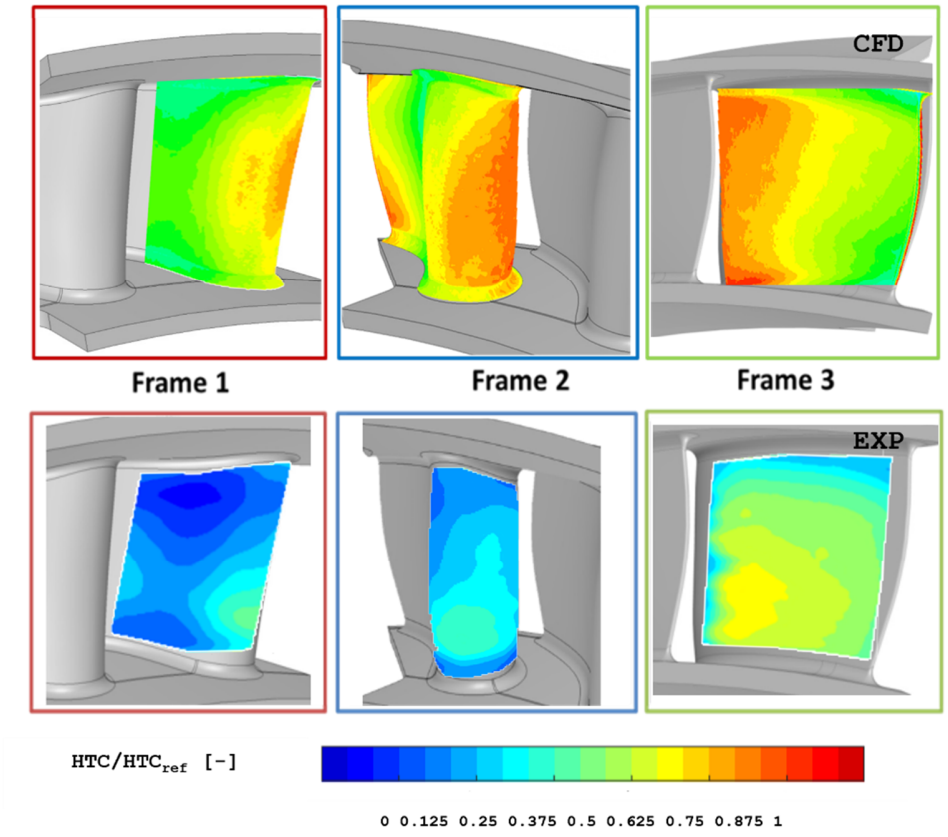

FIGURE 10: HEAT TRANSFER COEFFICIENT (© 2022 Baker Hughes Company – All rights reserved)

As a matter of fact, with reference to FIGURE 4, the lower half of the *LE* region is subjected to a higher flow incidence (positive swirl angle), whereas the opposite occurs on the higher half (negative swirl angle). This also dictates a higher *HTC* value on the lower than the higher span half, as also reported in previous works [17] [33].

Now moving to frame 1, the HTC is found to progressively decrease and then reaugment where flow is accelerated towards the throat section. In addition, *HTC* is reduced in the proximity of both inner and outer endwalls, where flow velocities are lower. For what regards *CFD* results, these qualitatively resembles measurements, but fail in providing a satisfactory match from the quantitative standpoint (note the colorbar change between exp and CFD results).

In fact, a similar twisted stagnation line can be observed on the airfoil *LE*, while it does not show the higher/lower *HTC* value respectively in the lower/higher span half region, in great disagreement with the experimental maps. Moreover, a gradual reduction and reaugmentation of the *HTC* is found as well by *CFD* on the *PS* surface, where also lower *HTC* zones are present close to the inner and outer endwalls, even if the radial gradient is underpredicted with respect to measurements. It is to be noted, however, that the numerical results on frame 1 and 2 clearly shows that a non-perfect periodic behaviour of the flow field investing the two airfoils is predicted by *CFD*, in contrast to what has been measured in the rig.

In turns, the two airfoils have not the same *HTC* at the nose. As previously pointed out, quantitative values on LE and PS are significantly overpredicted by CFD; on the other hand they fall on much more comparable values on the back part of the SS (frame 3), after transition occurs. However the predicted pattern is quite different, as higher heat transfer coefficient values are generally measured in the outer part of such a surface, opposite to what is evidenced by experiments.

Unfortunately, this is a further indicator of the inaccuracy of the present numerical technique. With an analogue fashion to FIGURE 10, FIGURE 11 reports the contours of adiabatic wall temperature non-dimensionalized ($T_{aw,nd}$) as per Eq. (4), where T_{aw} is substituted to T_t. The experimental maps of adiabatic wall temperature clearly show a quasi one-dimensional distribution as function of the radial coordinate. The maximum adiabatic wall temperature is found close to the midspan, yet slightly moved radially inward. Moreover, some intensity reduction with respect to $T_{t,nd}$ at Plane 40 (see FIGURE 4 for reference) is found as associated to the transient nature of the present test and majorly due to the heat dispersion within the rig.

The hot streak around the mid span fraction and the cold "trails" at both inner and outer radii follow the same distribution found at Plane 40 up to the airfoil *LE* and keep coherent also along the *SS* surface, whereas a non-negligible temperature decrease occurs on the *PS*, where flows tend to detach from, thus promoting mixing.

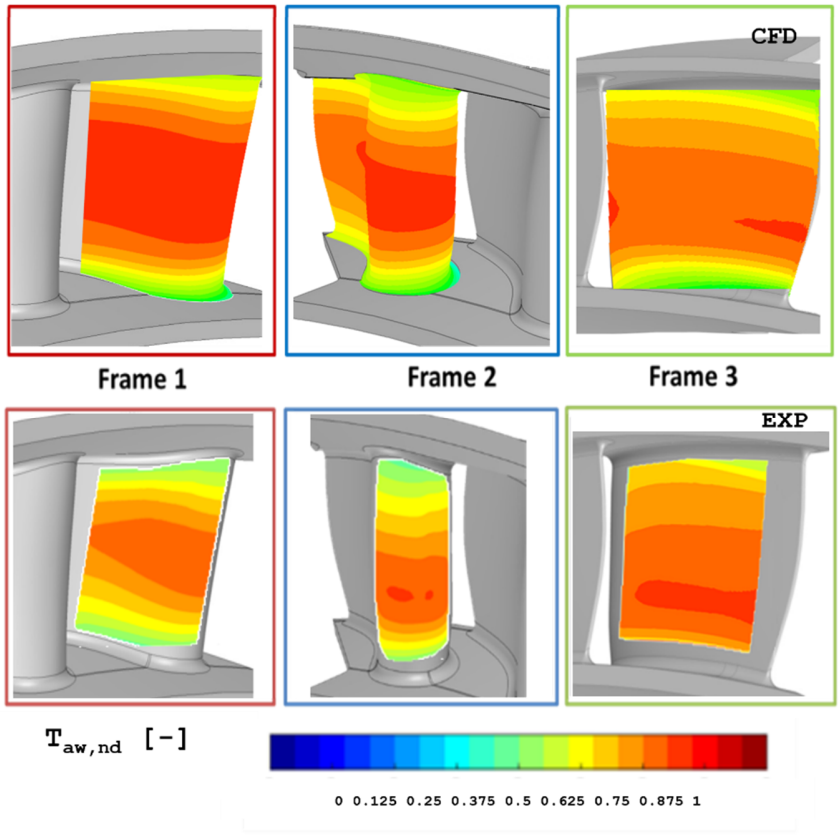

FIGURE 11: ADIABATIC WALL TEMPERATURE (© 2022 Baker Hughes Company – All rights reserved)

This is partly replicated also by *CFD* results, with a better match on the airfoil *LE* and *PS* surface. The hot streak on the suction surface is thinned, moving downstream, which does not seem to occur for experimental , indicating an overprediction of hot streak temperature. Overall the maximum adiabatic wall temperature is higher than the experimental results, mainly because transient heat losses are present for numerical results.

CONCLUSIONS

This paper describes an experimental test case with a combustor simulator and a nozzle cascade, where both adiabatic effectiveness and *HTC* measurements have been carried out, together with comparative numerical simulations.

The film cooling system has been fully modeled, whereas the heat transfer coefficient has been derived through the two-point method, conventionally employed in gas turbine applications. The objective was to judge the capability of traditional *RANS* modeling approaches in characterizing both film effectiveness and heat transfer.

The film-cooling behaviour has been experimentally retrieved by means of *PSP* measurements, showing that the cooling jets are drastically influenced by the high-swirl impacting main flow. In fact, coolant traces are found to be accumulated towards the midspan on the airfoil *PS*, while they are conveyed within the lower half span on the *SS*. *CFD* is partially capable of describing the same phenomena, but still some improvement margin exists, which could be attained via more advanced modelling techniques.

For what regards the *HTC*, derived via transient *IR* measurements on the rig, its distribution on the airfoil surface is strictly dictated by the inlet swirl profile, which not only induces a twisted stagnation line on the airfoil *LE* but also implies a non-uniform radial distribution on both pressure and suction sides. *RANS* modelling returns only qualitatively comparable results as compared to test data, although it fails to provide an acceptable quantitative assessment which results in high discrepancies.

As a whole, this work shows that conventional/industrial approaches might be used for addressing a preliminary design of *HPT* nozzle guide vanes even in the presence of highly unsteady combustor outflows. However, more advanced, yet time-consuming, *CFD* methods shall be strongly considered for assessing heat loads, since the impact on components lifespan could be non-negligible.

ACKNOWLEDGEMENTS

Regione Toscana and Baker Hughes are acknowledged respectively as co-funder and coordinator partner of the STech ‘Smart Technologies’ program 2017-2019 (FAR-FAS 2014 public notice), within which the combustor simulator test rig was developed. Baker Hughes is also thanked for the possibility to publish the present results.

REFERENCES

[1] R. Stabe, W. Whitney and T. Moffitt, "Performance of a high-work low aspect ratio turbine tested with a realistic inlet radial temperature profile," in *20th Joint Propulsion Conference, American Institute of Aeronautics and Astronautics*, 1991.

[2] T. L. Butler, O. P. Sharma, H. D. Joslyn and R. P. Dring, "Redistribution of an inlet temperature distortion in an axial flow turbine stage," *Journal of Propulsion and Power,* p. 5:64–71, 1989.

[3] T. Shang, G. Guenette, A. Epstein and A. Saxer, "The influence of inlet temperature distortion on rotor heat transfer in a transonic turbine," in *31st Joint Propulsion Conference and Exhibit, American Institute of Aeronautics and Astronautics*, 1995.

[4] M. D. Barringer, K. A. Thole and M. D. Polanka, "Experimental evaluation of an inlet profile generator for high pressure turbine tests," in *Proceedings of the ASME Turbo Expo 2006 - Power for Land, Sea, and Air*, 2006.

[5] S. C. Jenkins and D. G. Bogard, "Superposition Predictions of the Reduction of Hot Streaks by Coolant From a Film-Cooled Guide Vane," *Journal of Turbomachinery,* vol. 131, 2009.

[6] K. S. Chana, J. R. Hurrion and T. V. Jones, "The Design, Development and Testing of a Non-Uniform Inlet Temperature Generator for the QinetiQ Transient Turbine Research Facility," *American Society of Mechanical Engineers Digital Collection,* p. 273–80, 2003.

[7] S. Jacobi, C. Mazzoni, K. Chana and B. Rosic, "Investigation of Unsteady Flow Phenomena in First Vane Caused by Combustor Flow With Swirl," *American Society of Mechanical Engineers Digital Collection,* 2016.

[8] I. Qureshi, A. Beretta and T. Povey, "Effect of Simulated Combustor Temperature Nonuniformity on HP Vane and End Wall Heat Transfer: An Experimental and Computational Investigation," *Journal of Engineering for Gas Turbines and Power,* vol. 133, 2011.

[9] S. Salvadori, F. Montomoli, F. Martelli, K. S. Chana, I. Qureshi and T. Povery, "Analysis on the Effect of a Nonuniform Inlet Profile on Heat Transfer and Fluid Flow in Turbine Stages," *Journal of Turbomachinery,* vol. 134, 2012.

[10] A. Krichbaum, H. Werschnik, M. Wilhelm, H. P. Schiffer and K. Lehmann, "A Large Scale Turbine Test Rig for the Investigation of High Pressure Turbine Aerodynamics and Heat Transfer With Variable Inflow Conditions," *American Society of Mechanical Engineers Digital Collection,* 2015.

[11] C. M. Cha, S. Hong, P. T. Ireland, P. Denman and V. Savarianandam, "Experimental and Numerical Investigation of Combustor-Turbine Interaction Using an Isothermal Nonreacting Tracer," *Journal of Engineering for Gas Turbines and Power,* p. 134(8), 2012.

[12] C. M. Cha, P. T. Ireland, P. A. Denman and V.

Savarianandam, "Turbulence Levels Are High at the Combustor-Turbine Interface," in *Turbo Expo: Power for Land, Sea and Air*, 2012.

[13] T. Shih and Y.-L. Lin, "Controlling secondary-flow structure by leading-edge airfoil fillet and inlet swirl to reduce aerodynamic loss and surface heat transfer," *J. Turbomach.,* vol. 125, no. 1, pp. 48-56, 2003.

[14] Y.-L. Lin, H. J. Schock, T. I. Shih and R. S. Bunker, "Effects of Inlet Swirl Angle on Flow and Heat Transfer in Contoured Turbine Nozzle Guide Vanes," *ASME International Mechanical Engineering Congress and Exposition,* vol. 35623, no. 279-288, 2001.

[15] L. Giller and H. P. Schiffer, "Interactions between the Combustor Swirl and the High Pressure Stator of a Turbine," in *Turbo Expo: Power for Land, Sea and Air*, 2012.

[16] H. Werschnik, J. Hilgert, M. Wilhelm, M. Bruschewski and H. P. Schiffer, "Influence of Combustor Swirl on Endwall Heat Transfer and Film Cooling Effectiveness at the Large Scale Turbine Rig," *Journal of Turbomachinery,* vol. 139, no. 8, pp. 1-12, 2017.

[17] I. Qureshi, A. Smith and T. Povery, "HP Vane Aerodynamics and Heat Transfer in the Presence of Aggressive Inlet Swirl," *Journal of Turbomachinery,* vol. 135, no. 2, 2012.

[18] C. Battisti, F. Kost, N. Atkins, W. Playford, M. Orain, G. Caciolli, L. Tarchi, M. Mersinligil and J. Raffel, "Full Aerothermal Combustor Turbine Interaction Research," in *Proceedings of the EASN workshop on Flight Physics and Propulsion*, 2012.

[19] C. Koupper, G. Caciolli, L. Gicquel, F. Duchaine, G. Bonneau and L. Tarchi, "Development of an Engine Representative Combustor Simulator Dedicated to Hot Streak Generation," *Journal of Turbomachinery,* vol. 136, 2014.

[20] T. Bacci, R. Becchi, A. Picchi and B. Facchini, "Adiabatic Effectiveness on High-Pressure Turbine Nozzle Guide Vanes Under Realistic Swirling Conditions," *Journal of Turbomachinery,* vol. 141, 2019.

[21] F. Duchaine, J. Dombard, L. Gicquel and C. Koupper, "On the importance of inlet boundary conditions for aerothermal predictions of turbine stages with large eddy simulation," *Computers & Fluids,* p. 154:60–73, 2017.

[22] A. Andreini, T. Bacci, M. Insinna, L. Mazzei and S. Salvadori, "Modelling strategies for the prediction of hot streak generation in lean burn aeroengine combustors," *Aerospace Science and Technology,* p. 79:266–77, 2018.

[23] S. Cubeda, L. Mazzei, T. Bacci and A. Andreini, "Impact of Predicted Combustor Outlet Conditions on the Aerothermal Performance of Film-Cooled High Pressure Turbine Vanes," *Journal of Engineering for Gas Turbines and Power,* pp. 141:051011-051011–7, 2019.

[24] S. Cubeda, T. Bacci, L. Mazzei, S. Salvadori, B. Facchini, L. Fiorineschi and Y. Volpe, "Design of a Non-Reactive Warm Rig with Real Lean-Premixed Combustor Swirlers and Film-Cooled First Stage Nozzles," in *Proceedings of ASME Turbo Expo (GT2020-14186)*, 2020.

[25] T. Bacci, A. Picchi, G. Babazzi, B. Facchini and S. Cubeda, "Heat Transfer Coefficient and Adiabatic Wall Temperature Measurements on a High-Pressure Turbine Nozzle Guide Vane with Representative Inlet Swirl and Temperature Distortions," in *Proceedings of ASME Turbo Expo (GT2022-81263)*, 2022.

[26] G. Babazzi, T. Bacci, A. Picchi, B. Facchini and S. Cubeda, "Film Cooling and Cold Streaks Tracking on a Fully Cooled Nozzle Guide Vane Under Representative Combustor Outflow Conditions," in *Proceedings of ASME Turbo Expo (GT2022-81360)*, 2022.

[27] B. F. Hall, K. S. Chana and T. Povey, "Design of a Non Reacting Combustor Simulator with Swirl and Temperature Distortin with Experimental Validation," in *Proceedings of ASME Turbo Expo (GT2013-95499)*, 2013.

[28] T. Bacci, G. Caciolli, B. Facchini, L. Tarchi, C. Koupper and J. L. Champion, "Flowfield and Temperature Profiles of a Combustor Simulator Dedicated to Hot Streaks Generation," in *Proceedings of ASME Turbo Expo (GT2015-42217)*, 2015.

[29] T. Bacci, A. Picchi, B. Facchini and S. Cubeda, "A New Experimental Approach for Heat Transfer Coefficient and Adiabatic Wall Temperature Measurements on a Nozzle Guide Vane with Inlet Temperature Distortions," *Journal of Turbomachinery,* vol. 144(3):031007, 2022.

[30] F. R. Menter, "Best Practice: Scale Resolving Simulations in ANSYS CFD," *ANSYS Germany GmbH,* 2015.

[31] D. Griffini, M. Insinna, S. Salvadori and F. Martelli, "Clocking Effects of Inlet Nonuniformities in a Fully Cooled High-Pressure Vane: A Conjugate Heat Transfer Analysis," *Journal of Turbomachinery,* vol. 138, 2016.

[32] S. Cubeda, L. Mazzei and A. Andreini, "External heat transfer on nozzle guide vanes under highly swirled combustor outlet flow," *13 th European Conference on Turbomachinery Fluid dynamics & Thermodynamics. EUROPEAN TURBOMACHINERY SOCIETY,* Vols. (ETC2019-293), no. 2019.

[33] F. Shaikh and B. Rosic, "Unsteady Phenomena at the Combustor-Turbine Interface," *Journal of the Global Power and Propulsion Society,* pp. 5:202-215, 2021.

